Electrostatically driven interaction of silica-supported lipid bilayer nanoplatforms and a nerve growth factor-mimicking peptide

ARTICLE *in* SOFT MATTER · MAY 2013

Impact Factor: 4.03 · DOI: 10.1039/C3SM50628B

7 AUTHORS, INCLUDING:

Cristina Satriano
University of Catania
61 PUBLICATIONS **1,080** CITATIONS
SEE PROFILE

Diego La Mendola
Università di Pisa
51 PUBLICATIONS **702** CITATIONS
SEE PROFILE

Luca Prodi
University of Bologna
207 PUBLICATIONS **7,056** CITATIONS
SEE PROFILE

Enrico Rizzarelli
University of Catania
290 PUBLICATIONS **6,097** CITATIONS
SEE PROFILE

Soft Matter

RSC Publishing

PAPER

View Article Online
View Journal

Electrostatically driven interaction of silica-supported lipid bilayer nanoplatforms and a nerve growth factor-mimicking peptide†

Cite this: DOI: 10.1039/c3sm50628b

Alessio Travaglia,‡[a] Cristina Satriano,*[a] Maria Laura Giuffrida,[b] Diego La Mendola,[c] Enrico Rampazzo,[d] Luca Prodi[d] and Enrico Rizzarelli[ab]

Received 2nd March 2013
Accepted 12th March 2013

DOI: 10.1039/c3sm50628b

www.rsc.org/softmatter

The interaction between lipid vesicles and NGF(1–14) peptide, mimicking nerve growth factor, was addressed to fabricate peptide-associated supported lipid bilayers (SLBs). According to a model of predominant electrostatic interactions, zwitterionic and anionic lipid vesicles were used to optimize the peptide association with the lipid membranes. Both planar silica and core–shell nanoparticles (NPs) were used as polar hydrophilic substrates to form the SLBs functionalized with the NGF peptide. The hybrid biointerface was scrutinized by a multitechnique approach with QCM-D, FRAP and fluorescence spectroscopy in terms of self-assembling kinetics, lipid lateral diffusion, and energy transfer processes in the SLB-wrapped silica NPs dye-doped in the core. The response of neuronal cells to the NGF(1–14)-SLBs highlighted their promising application as a drug delivery nanoplatform for ageing-related diseases.

1 Introduction

The immobilization of biomolecules on solid nanoplatforms for transport and smart release is a highly challenging topic to overcome present limitations in drug delivery. The common strategy, among those currently used for cell targeting, is based on *rigid* gel-phase vesicles, which comprise a lipid bilayer surrounding an aqueous core.[1]

A novel approach has been recently proposed, where a supported lipid bilayer (SLB) is formed *via* fusion of liposomes to a porous silica nanoparticle (NP).[2] Such versatile hybrid nanocarrier (NP–SLB) synergistically combines features of both mesoporous silica particles and liposomes, thus exhibiting many features of an ideal targeted therapeutic delivery platform. The high pore volume and surface area of the spherical porous silica core allow for an enormous encapsulation capacity for a spectrum of molecules. The *fluid*-phase lipid bilayer decorating the outer surface of the nanoparticle serves as a modular, reconfigurable scaffold, enabling the attachment of a variety of molecules for cell-specific targeting.[3]

In vitro experiments proved the stability of the SLB acting as a capping system by sealing of colloidal mesoporous silica nanoparticles, thus enabling a tunable release-on-demand of the adsorbed molecules.[4] Moreover, the capability of lipid molecules to freely diffuse within the SLB provides high delivery efficiency and enhances targeting specificity, also with a minimal number of targeting ligands.[5] Finally, SLB-based nanoplatforms can be functionalized with biomolecules, either *via* covalent and/or physical binding. The latter approach offers a tunable and reversible adsorption/release by proper matching of the physicochemical properties of both the substrate and the ligand molecules, including the charge and hydrophilic character.[6,7]

The biomolecule of interest in the present study is the peptide sequence named NGF(1–14), which encompasses the N-terminal domain of nerve growth factor (NGF).[8] NGF is a protein involved in the development, maintenance and survival of the nervous system.[9] Recently, NGF has gained interest as a therapeutic agent for neurological pathologies such as Alzheimer's disease (AD).[10]

Current approaches for NGF delivery include invasive methods, such as intracerebral injections and implantation of viral vectors, as well as intranasal delivery and topical ocular applications, which are less invasive but still require improvements.[11] Encapsulation of NGF into micro- and nanoparticles such as liposomes to prevent enzymatic degradation and, through surface functionalization of the carrier, to promote its permeability across the blood–brain barrier has been reported.[12]

Whether encapsulated or not, NGF binds to two distinct classes of receptors: TrkA (tropomyosin receptor kinase) and the p75 receptor, which transmit respectively pro-survival and apoptotic signals, the latter being responsible for adverse side effects.[13,14]

[a]Department of Chemical Sciences, University of Catania, viale Andrea Doria, 6, 95125 Catania, Italy. E-mail: csatriano@unict.it; Fax: +39 095 580138; Tel: +39 095 738 5136
[b]Institute of Biostructures and Bioimages, Catania National Council of Research (CNR), viale Andrea Doria, 6, 95125 Catania, Italy
[c]Department of Pharmacy, University of Pisa, via Bonanno Pisano 6, 56100, Pisa, Italy
[d]"G. Ciamician" Department of Chemistry, University of Bologna, Via Selmi 2, 40126 Bologna, Italy

† Electronic supplementary information (ESI) available: (S1) Peptide loading efficiency determination; (S2) kinetic curves of fluorescence recovery for FRAP experiments. See DOI: 10.1039/c3sm50628b

‡ Present address: Center for Neural Science, New York University, 4 Washington Place, New York, NY 10003, USA.

Promising results have been obtained with the use of peptide fragments able to mimic the NGF activities while preventing unwanted adverse effects on non-target regions or cells.[15] A major advantage of this approach is the tuning ability for the desired properties by proper sequence design. The N-terminal domain of NGF is crucial and specific to bind and activate only the TrkA receptor.[16] Accordingly, the NGF(1–14) peptide, at micromolar concentrations, has been demonstrated to exhibit good pro-survival effects in neuronal cells.[8]

The peptide association to the SLB might enable the improvement of its resistance to degradation and bioavailability, due to the synergic combination of materials and biophysical properties of the SLB-based nanoplatform.

Herein, we demonstrate a proof-of-concept approach in which the association of the NGF(1–14) peptide to lipid vesicles is tested on the basis of an electrostatic model. Since at the physiological pH the primary peptide sequence, SSSHPIFHRGEFSV, makes the molecules to bear an overall positive charge, vesicles prepared from zwitterionic 1-palmitoyl-2-oleoyl-*sn-glycero*-3-phosphocholine (POPC) and negatively charged 1-palmitoyl-2-oleoyl-*sn-glycero*-3-phospho-L-serine (POPS) lipids were used. The NGF(1–14)-supported lipid bilayers were obtained by vesicle adsorption on silica substrates, both 2D planar surfaces and 3D dye-doped core–shell nanoparticles. Such hybrid nanoplatforms were characterized using a multi-technique approach of physicochemical analyses, including Quartz Crystal Microbalance with Dissipation Monitoring (QCM-D), laser scanning confocal microscopy with Fluorescence Recovery After Photobleaching (FRAP), FT-IR, UV-visible and fluorescence spectroscopies, and studies on cellular viability and proliferative assays.

2 Experimental

2.1 NGF(1–14) synthesis and physicochemical characterization

The peptide fragment NGF(1–14), encompassing the 1–14 sequence of the human NGF amino-terminal domain, SSSHPIFHRGEFSV–NH_2, was synthesized with the C-termini amidated, as previously reported.[8] All amino acid residues were added according to the TBTU/HOBT/DIEA activation method in Fmoc chemistry on Fmoc-PAL-PEG resin.

The peptide has five protonation centers: the Ser-1 amino group (pK = 7.56), two imidazole groups of histidyl residues His-4 and His-8 (pK = 6.57 and pK = 6.01), the guanidine group of Arg-9 and the glutamyl γ-carboxylic function (pK = 4.13). The pK values reported were determined by means of potentiometric measurements.[8] The isoelectric point of 9 was calculated using Innovagen's Peptide Property Calculator.§

§ The net charge (Z) of the NGF(1–14) peptide at pH = 7.4 is 0.8 as estimated by the formula:

$$Z = \sum_i N_i \frac{10^{pK_{a_i}}}{10^{pH} + 10^{pk_{a_i}}} - \sum_j N_j \frac{10^{pH}}{10^{pH} + 10^{pK_{a_j}}}$$

where N_i is the number and pK_{a_i} is the pK_a value of the N-terminal groups and the side chains of Arginine and Histidine. The j-index pertains to the glutamic acid residue. The pK value of the guanidine group of Arg is 12.4.

The peptide was purified by means of a preparative reversed-phase high-performance liquid chromatography (rp-HPLC), and characterized by analytical rp-HPLC and ESI-MS (NGF-(1–14): [R_t = 26.10 min]. $C_{71}H_{103}N_{22}O_{20}$, calculated mass = 1584.73, ESI-MS [observed m/z: $(M + H)^+$ 1586.7; $(M + 2H)^{2+}$ 793.7]). Other experimental details have been reported elsewhere.[8]

2.2 Preparation of small unilamellar vesicle (SUV) dispersions

Small unilamellar vesicles (SUVs) were prepared from chloroform solutions of 1-palmitoyl-2-oleoyl-*sn-glycero*-3-phosphocholine (POPC) and 1-palmitoyl-2-oleoyl-*sn-glycero*-3-phospho-L-serine (sodium salt) (POPS) purchased from Avanti Polar Lipids (Alabaster, AL, USA). All other chemicals were purchased from Sigma-Aldrich (USA). Water was deionized (resistivity > 18 MΩ cm^{-1}) and purified using a Milli-Q unit (Milli-Q plus, Millipore, France). Phosphate Buffer Saline (PBS) solution was prepared from tablets (0.01 M phosphate buffer containing 0.003 M KCl and 0.14 M NaCl, pH 7.4). For the preparation of negatively charged bilayers, 10 mM $MgCl_2$ was added to the PBS buffer. The buffer was filtered and degassed.

Zwitterionic vesicles were prepared from pure POPC (hereafter called PC). Negatively charged vesicles were prepared from POPC/POPS in a 3 : 1 ratio (hereafter called PS25). As a fluorescent probe, rhodamine-DHPE (1,2-dihexadecanoyl-*sn-glycero*-3-phosphoethanolamine, Invitrogen, Carlsbad, CA, USA) was added (1 wt%) to 5 mg mL^{-1} solutions of lipid in a round bottomed flask. The solvent was evaporated under a flow of argon, while rotating the round-bottomed flask, to form a film on the wall of the flask. The lipid film was emulsified in buffer at room temperature, vortexed, and extruded 11 times through a 100 nm polycarbonate membrane, followed by another 11 times through a 30 nm membrane (Avanti Polar Lipids Inc., AL, US).

To prepare NGF(1–14)-SUV systems the membrane rehydration was accomplished with 600 μM NGF(1–14) in PBS. Vesicles prepared in this way typically measured 80–100 nm, as determined by dynamic light scattering. The refrigerated vesicle solutions were stored under Ar and used within two weeks, according to an established protocol.[6] Before the use, the size of SUVs was checked by light scattering measurements.

The peptide loading efficiency was assessed by centrifugation and spectrophotometric determinations (Fig S1 in the ESI†).

2.3 Silica-supported lipid bilayer formation and physicochemical characterization

SLBs were prepared by adsorption of the SUVs on polar hydrophilic silicon oxide surfaces, followed by vesicle rupture–fusion processes and the formation of a homogeneous silica supported lipid membrane.[17]

For adsorption experiments on the 2D silica surfaces the used substrates were QCM-D sensor crystals (5 MHz) reactively sputter-coated with 50 nm silicon oxide (QSense, Biolin Scientific, Finland), monopolished silica wafers (University Wafers, USA) for FT-IR measurements, glass bottom 96-well plates

(uncoated, γ-irradiated, MatTek Corporation, Ashland, MA, USA) for FRAP analysis and cellular experiments. Immediately before the experiments the surfaces were cleaned by 20 minutes of UV ozone treatment, multiple rinsings with ultrapure water and drying under an argon stream.

For the adsorption studies on the 3D surfaces, porous core–shell silica nanoparticles (NPs), dye-doped in the core with coumarin, were synthesized. Average NP dimensions were of 25 nm and 10 nm for external and internal diameters, respectively.[18]

For the physicochemical characterization and the cellular assays the vesicles, diluted to a final concentration of 0.1 mg mL^{-1}, were allowed to adsorb on the silica surfaces and then were rinsed with PBS buffer.

2.4 Fourier transform infrared spectroscopy (FT-IR)

FT-IR spectra were recorded on a Bruker Tensor 27 spectrophotometer, equipped with a room temperature DTGS detector, mid-IR source (4000 to 400 cm^{-1}), and a KBr beam splitter. Each spectrum was acquired at a resolution of 4 cm^{-1} (16 scans). Lipid vesicle dispersions were allowed to adsorb on freshly cleaned silicon dioxide surfaces. After 15 minutes of incubation the samples were washed by multiple rinsing with PBS and gently dried under a stream of Ar.

The reference 'thick' NGF(1–14) sample was prepared by drop casting of 600 μM peptide solution until the deposition of a visible film on the silicon dioxide surface.

2.5 Quartz crystal microbalance with dissipation monitoring (QCM-D)

QCM-D measurements were carried out in flow mode (50 μL min^{-1}) on a QSense E1 unit (Biolin Scientific, Finland). Prior to each measurement series, the sensor crystals were cleaned by immersion in 10 mM sodium dodecyl sulfate (SDS, >1 h), followed by rinsing with Millipore water (MQ), Ar blow dried and treated by UV-ozone (30 min). Further cleaning was performed *in situ* in the measurement cell by two subsequent steps of rinsing with MQ and SDS.

The fundamental, along with the third, fifth, seventh and ninth harmonic of the fundamental frequency, was monitored as a function of time to determine the change in frequency of the crystal. Frequency shifts were normalized by division by the overtone number (n). The dissipation change was also recorded as a function of time. The average of the frequency and dissipation change of the harmonics (n = 3–9) were averaged to estimate the error in the measurements.

2.6 Scanning confocal microscopy (LSM) and fluorescence recovery after photobleaching (FRAP)

LSM observations were carried out by using an Olympus FV1000 confocal laser scanning microscope equipped with multiline Ar and HeNe lasers, an oil immersion objective (60×O3 PLAPO) and a spectral filtering system. The excitation wavelength was set at 543 nm, and the emitted light was detected at 591 nm. The detector gain was fixed at a constant value and images were taken for all of the samples at random locations throughout the area of the well.

For FRAP investigations, time-solved snapshots were acquired as follows: three images before bleach, then bleaching by using a high intensity (95% power) Ar laser, and other micrographs every 5 seconds up to 2 minutes. By translating the sample stage, an average of 10 spots per substrate were photobleached in a given experiment.

Fluorescence recovery curves were analyzed by ImageJ software (FRAP Profiler macro). The data were normalized to the initial (pre-photobleach) value, which enabled the percentage of photobleaching and the percentage fluorescence recovery within the laser region to be determined. For each sample, the emission recorded from the bleached spots was compared with that coming from contiguous non-bleached areas.

2.7 UV-vis and fluorescence spectrophotometric measurements

Mother solutions in water of silica nanoparticles dye-doped with coumarin (NP) were diluted in 10 mM PBS (pH = 7.4 at 25 °C) at the final concentration of 2.7×10^{-6} M. Spectra were acquired upon progressive additions of SUVs, or SUV-NGF-(1–14), in molar ratios ranging from 10 : 1 to 1 : 10 (NPs to lipid dispersions).

Absorption spectra were recorded in the wavelength range of 200–700 nm with a JASCO V-560 UV-vis spectrophotometer equipped with a 1 cm path-length cell. Fluorescence spectra were recorded using a Cary Eclipse Fluorescence spectrophotometer with 0.5 nm resolution at room temperature. The emission was recorded at 90° with respect to the exciting line beam using 5:5 slit-widths for all measurements, λ_{ex} = 380 nm (for coumarin) and λ_{ex} = 540 nm (for rhodamine).

2.8 Cellular experiments

Human neuroblastoma SH-SY5Y cells were grown in DMEM-F-12 (1 : 1) medium, supplemented with 10% fetal bovine serum (FBS), 1% penicillin/streptomycin, 2 mM L-glutamine and maintained in a humidified incubator at 37 °C in 5% CO_2.

For LSM live cell imaging analysis, glass bottom 96-well plates were pre-coated with the different SLBs as well as NGF-(1–14). Cells were plated at a density of 1×10^5 in DMEM-F12 medium with 5% fetal bovine serum. After 24 hours cells were rinsed with PBS and stained with the lysosomal marker LysoTracker Green DND-26 (Molecular Probes, 1 μM in PBS) by 15 min treatment at 37 °C in 5% CO_2. After that, cells were rinsed with fresh PBS and observed using the confocal microscope.

Cell proliferation assay were performed by short incubation (6 h) of cells in essential medium, *i.e.*, in the absence of nutrients such as growth factors and serum, followed by 24 hours of incubation in a medium supplemented with 5% FBS. Optical microscopy observations were performed using a Leica DMI 4000 B microscope. Cells were counted from the images taken on three random fields from each sample in triplicate with the tool provided by ImageJ software. Statistical significance was assessed by comparison of mean values by one-way analysis of variance (ANOVA).

3 Results and discussion

In Scheme 1 a simplified scenario of peptide–lipid association to SUV and SLB is sketched.

Indeed, whereas the hydrophobic character of the peptide would favor an intramembrane configuration, the predominance of hydrophilic and/or charged residues in the sequence will result in the peptide molecules associated with the outer and inner polar heads of the bilayer. In the present case the NGF(1–14) peptide, which is hydrophilic and positively charged at the pH used in the experiment, predominantly resides in the vesicle inner volume and on the outer shell of the vesicles, especially for the negatively charged lipids (Scheme 1A). The adsorption of SUV-NGF(1–14) on the silica supports will result in a SLB nanoplatform with NGF(1–14) peptide molecules associated with the polar lipid heads of the membrane (Scheme 1B). It has to be noted that the calculated peptide charge of 0.8§ derives from the averaged p*K* values of the peptide protonation centers. At physiological pH the most part of peptide molecules carry a net positive charge of +1 on the amino group.

The successful peptide association to the lipid vesicles and subsequently to the lipid adlayers on the silica surfaces was assessed by FTIR analyses. Fig. 1 shows for both zwitterionic and the negatively charged lipids the characteristic peaks at 2920 cm^{-1} (CH_2 anti-symmetric stretching) and at 2850 cm^{-1} (CH_2 symmetric stretching), as well as a broad band in the region of 3000–3700 cm^{-1}, due to phosphate groups and hydroxyl stretching.[19]

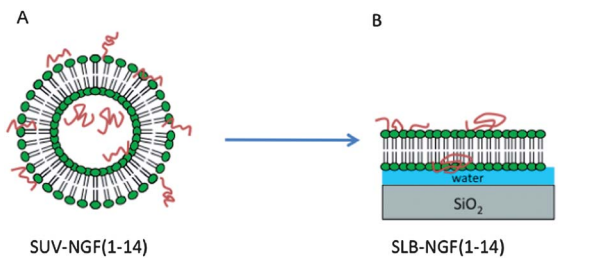

Scheme 1 Graphical representation of peptide–lipid association to the SUV (A) and the following NGF peptide-SLB (B).

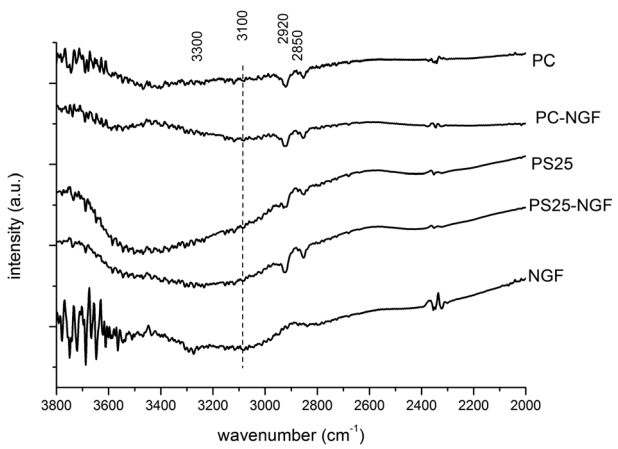

Fig. 1 FTIR spectra of zwitterionic (PC) and negatively charged (PS25) lipid adlayers, the corresponding peptide-associated PC-NGF(1–14) and PS25-NGF-(1–14) and control NGF(1–14) adlayers.

The NGF(1–14) spectrum exhibits a peak at 3300 cm^{-1}, attributed to the absorption of water molecules as well as to the contribution from the amide bonds and a band at 3000–3100 cm^{-1}, assigned to C=C–H asymmetric stretch of the aromatic rings of the phenylalanine residues.[20]

The spectra of NGF(1–14)-loaded PC and PS25 clearly exhibit spectral features from both the lipid and the peptide, as especially evident in the 3000–3100 cm^{-1} region, thus confirming the successful association of the peptide to the lipid adlayers.

QCM-D and FRAP techniques were used to investigate the adsorption processes of NGF(1–14)-loaded SUVs on planar silica surfaces.

In the QCM-D instrument, the quartz crystal sensor is mechanically excited into a resonance by applying an alternating potential across two conducting films deposited on either side of the quartz crystal. The frequency, f, of this oscillation is sensitive to the amount of adsorbed materials on the crystal surface. In addition to the frequency, a second parameter is monitored, that is the dissipation, D, or energy loss in the molecular film on the sensor. This is measured by turning off the voltage to the sensor, which causes the oscillation to decay. The decay rate is related to the elasticity and viscosity, or structure, of the molecular layer on the sensor. QCM-D, providing information about the mass and the conformational changes of the adsorbed material, has been shown to be a useful tool to study the formation of SLBs.[21]

The QCM-D response observed when adsorbing SUVs made of zwitterionic lipids or negatively charged lipids (in the presence of divalent ions, including Ca^{2+} or Mg^{2+} (ref. 22)) on silica shows a two-phase process. The first phase reflects the adsorption of a vesicular layer of elevated coverage until a minimum in frequency (Δf_{min}) and a maximum in dissipation (ΔD_{min}) are reached. The second phase corresponds to vesicle rupture–fusion processes with the formation of a continuous SLB. Typical values of $\Delta f_{fin} \sim -26$ Hz and $\Delta D_{fin} < 0.5 \times 10^{-6}$ correspond to the formation of a continuous hydrated SLB.[17,20–23]

In Fig. 2 the QCM-D curves of Δf and ΔD are shown for the adsorption of control SUV and NGF(1–14)-SUV, either zwitterionic (Fig. 2a and b) or negatively charged (Fig. 2c and d) lipids.

All the vesicle solutions show the typical curve trends corresponding to the formation of a homogeneous SLB.

It is interesting to note that the kinetic curves of PC (Fig. 2a) and PC-NGF(1–14) (Fig. 2b) do not display any significant difference. On the other hand, the bilayer formation is slightly slowed down (of about 20 s) for PS25-NGF(1–14) (Fig. 2d) compared to the bare, negatively charged, PS25 (Fig. 2c).

The lateral mobility of the SLB at the interface with the 2D silica surfaces was analysed by performing FRAP experiments to scrutinize any possible perturbation in the lateral diffusion properties of the membrane induced by the presence of the NGF(1–14) peptide.

In Fig. 3 FRAP results indicate that both PC (Fig. 3a) and PC-NGF(1–14) (Fig. 3b) vesicles form fluid supported membranes,

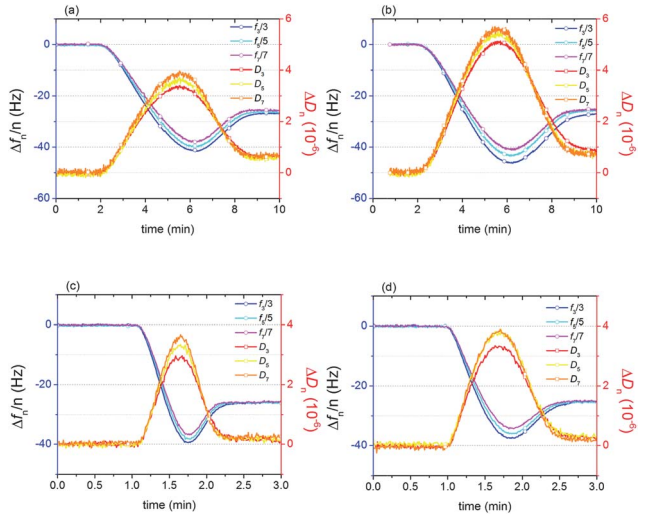

Fig. 2 QCM-D curves of Δf and ΔD corresponding to three overtones ($n = 3$, 5, and 7) for vesicle adsorption on 2D silica surfaces. Experiments performed in phosphate buffer saline (PBS) solution (pH = 7.4) for PC (a) and PC-NGF(1–14) (b) or in 10 mM $MgCl_2$ added PBS for PS25 (c) and PS25-NGF(1–14) (d).

which are able to fully recover from the quenching of fluorescence. Indeed, notwithstanding the visible presence of lipid aggregates (brighter regions) in the PC-NGF(1–14) membrane, the diffusion coefficient, calculated by using the Axelrod's algorithm[24] ($D_{coeff} = 0.88w_2/4\tau_{1/2}$, where w is the radius of the bleached area and $\tau_{1/2}$ describes time for 50% recovery), is 1.8 ± 0.1 μm^2 s^{-1} for both PC and PC-NGF(1–14).

Comparable results were obtained for PS25 and PS25-NGF(1–14) SLBs (images not shown). The calculated values for the diffusion coefficient are similar, with $D_{coeff} = 1.0 \pm 0.1$ μm^2 s^{-1} for PS25 and $D_{coeff} = 0.9 \pm 0.3$ μm^2 s^{-1} for PS25-NGF(1–14) SLB. The higher standard deviation measured for the latter highlights a stronger interaction between the NGF(1–14) peptide and the negatively charged lipid membrane than in the case of zwitterionic lipids.

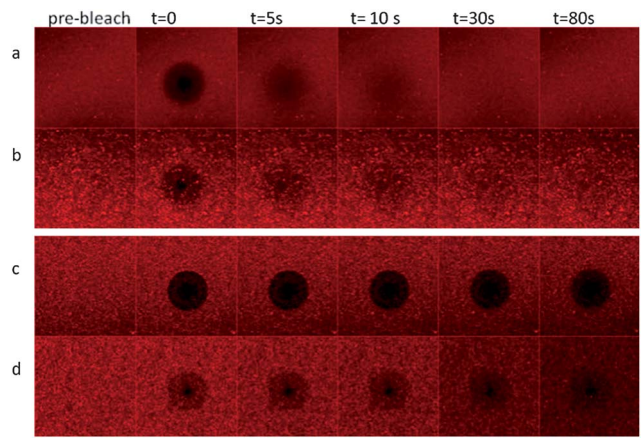

Fig. 3 Confocal microscopy images for FRAP experiments on: (a) PC SLB; (b) PC-NGF(1–14) SLB; (c) PS25 adlayer and (d) PS25-NGF(1–14) adlayer. Time-lapse images are shown for pre-bleach, immediately after bleach and 5 s, 10 s, 30 s and 80 s after bleach.

It has to be noted that the measured values of the diffusion coefficients are in agreement with the values reported for individual lipid molecules that freely laterally diffuse within the membrane.[25,26] The fact that NGF(1–14) molecules do not perturb the mobility of the SLBs can therefore be explained as due to the predominant peptide association to the lipid polar heads instead of the hydrophobic moieties of the membrane.

Furthermore, the lipid adlayers formed by adsorption in the absence of divalent cations of the negatively charged PS25 and NGF(1–14)-PS25 SUVs exhibit very different behaviours in the FRAP experiment. In fact, no recovery is apparent for PS25 (Fig. 3c) whereas a partial recovery of fluorescence is obtained for the PS25-NGF(1–14) adlayer (Fig. 3d). Thus the presence of the peptide prompts the formation of a mixed adlayer where the fraction of mobile lipids, likely as patches of SLB, is significantly higher than in the corresponding bare PS25. The kinetic curves for fluorescence recovery are discussed in detail in the ESI (see Fig. S2 in the ESI†).

Preliminary measurements of the interaction with the different lipid-based nanoplatforms were performed with neuroblastoma cells (SH-SY5Y) in order to assess: (i) the suitability of the used substrates as adhesive and non-toxic supports for cells, (ii) if any, cellular morphological differences for the NGF-functionalized SLBs with respect to the control bare ones.

Different levels of interaction between cells (in green, due to cellular staining of lysosomes) and the different SLBs (in red, due to lipid staining with rhodamine) are shown in Fig. 4.

First of all, according to QCM-D and FRAP results, a lipid membrane, more or less defective, is visible underneath the adhered cells for both zwitterionic and negatively charged lipids (clearly discernible patches of lipid membranes for PS25-NGF).

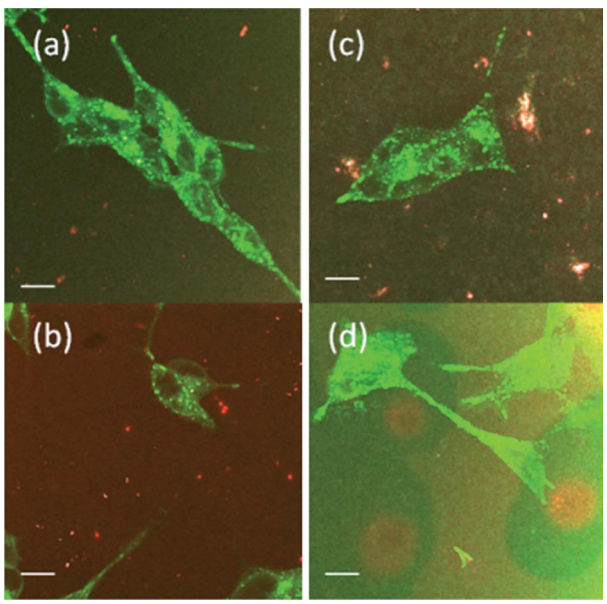

Fig. 4 Fluorescence merged channels of green ($\lambda_{ex}/\lambda_{em} = 488/519$ nm) and red ($\lambda_{ex}/\lambda_{em} = 543/591$ nm) from confocal microscopy live cell imaging of SH-SY5Y on SLBs made from: (a) PC, (b) PC-NGF(1–14), (c) PS25, and (d) PS25-NGF(1–14). Scale bar = 10 μm.

Secondly, cellular morphology evidences a good adhesion and the cellular survival is not compromised for any of the investigated conditions of lipid charge. Moreover, the overall cellular aspect indicates a lack of ameliorate for PC-NGF(1–14) (Fig. 4b) with respect to the bare zwitterionic one (Fig. 4a), but an evident improvement for PS25-NGF(1–14) (Fig. 4d) in comparison with the negatively charged PS25 (Fig. 4c).

Neurotrophins and their receptors are known to be involved both in proliferation and survival processes of various cells, either neuronal or non-neuronal, in physiological as well as pathologic conditions.

The proliferative effect of the NGF(1–14) peptide alone and that associated with the SLB, either zwitterionic PC or negatively charged PS25, was tested and the results are shown in Fig. 5.

Cells plated on NGF(1–14) pre-adsorbed on the glass show an increased number with respect to the control bare glass, in agreement with previously reported data of NGF(1–14) proliferative activity on SH-SY5Y cells.[8]

On the other hand, the poor adhesive properties of negative and zwitterionic SLBs towards neuronal cells[27] exhibit an improvement in PC-NGF(1–14) and even more in PS25-NGF-(1–14), indicating that the peptide maintains its activity in the hybrid NGF(1–14)-SLB nanoplatform.

This finding highlights the availability of peptide molecules at the outer surface of the supported membrane (as represented in Scheme 1) to interact with cells.

The implementation of the above-described systems from model 2D silica surfaces to core–shell 3D nanoparticles was investigated by the use of porous silica nanoparticles (NPs) doped in the core with coumarin dye molecules.[18,28] This dye was selected in order to have a high integral overlap, according to the Förster theory,[29] with the rhodamine dye used to stain the lipid as previously discussed. With this architecture, an energy transfer process from the coumarine to the rhodamine was expected provided a rather short (<10 nm) distance between the two fluorophores.[30]

Fluorescence measurements for the interaction of NGF-(1–14)-loaded SUVs (both zwitterionic and negatively charged) were thus carried out. Fig. 6 shows a decrease of the coumarin emission (at 475 nm) and a corresponding increase of rhodamine emission (at 590 nm) by progressive additions of PS25-NGF(1–14) SUVs to the silica nanoparticles.

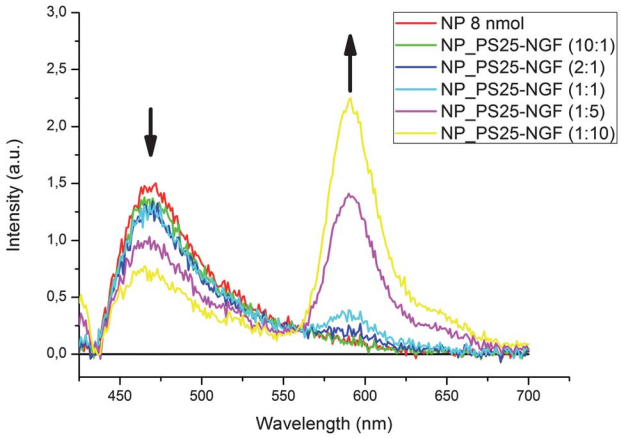

Fig. 6 Emission spectra (λ_{ex} = 380 nm) of a 2.7 μM NP solution in 10 mM $MgCl_2$ added-PBS for successive additions of PS25-NGF(1–14) vesicles in molar ratios ranging from 10 : 1 to 1 : 10.

The intensity values corrected for taking into account both inner filter effects and concentration changes[31] show that the decrease of the coumarin emission is not due to these artefacts, while the increase of the rhodamine emission cannot be completely explained in term of its concentration increase.

Such a finding points to an energy transfer process, indicative of a close distance between the two fluorophores. This is likely due to the SLB wrapping the silica nanoparticles. Moreover, we would like to underline that the coumarin moieties are covalently linked to the silica core, so that the effect cannot be due to dye leakage. It is noteworthy that such a surface decoration of the silica nanoparticles is a process that can modify the possible interaction between nanoparticles and cells, including cell internalization.[28] These findings suggest potential applications of the newly developed nanoplatforms in drug delivery and imaging (theranostics).

In this respect, it has to be stressed that the model of peptide association to the lipid membrane represented in Scheme 1 is a simplified representation that takes into account the predominant role of electrostatics and polar forces in the peptide–membrane interaction. Further studies, both experimental and theoretical molecular dynamic simulations, are in progress to fully address where does the peptide reside in the membrane and how its bioavailability and activity in the release might be triggered by proper tuning of lipid charge and composition.

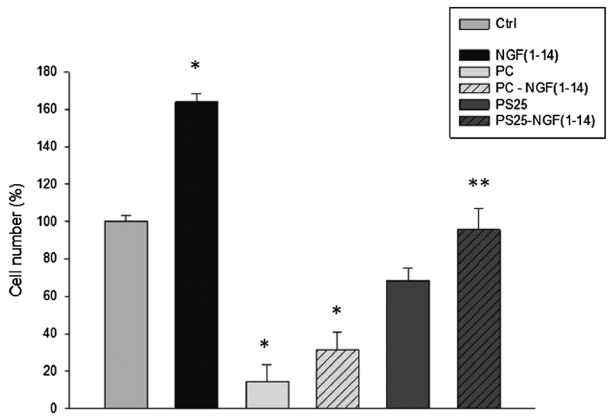

Fig. 5 Number of SH-SY5Y cells normalized to the control (bare glass) after 24 h of incubation time on SLB pre-coated surfaces. Bars represent standard error of means. (* = $p < 0.05$ w.r.t. control, ** = $p < 0.05$ w.r.t. PS25, One-way Anova test).

4 Conclusions

In summary, NGF peptide-functionalized supported lipid bilayers were successfully obtained by physical adsorption of NGF(1–14)-associated lipid vesicles on silica surfaces, both planar and core–shell nanoparticles. The characterization by the real-time detection of frequency and dissipation curves in QCM-D during the processes of vesicle adsorption and formation of a homogeneous supported lipid membrane evidenced a

minor perturbation in the viscoelastic properties of the SLB induced by the presence of the peptide. The characteristic lipid lateral diffusion within the supported membrane, as assessed by fluorescence recovery after photobleaching analyses, confirmed the maintenance of the fluidity property of the supported membrane functionalized with the NGF peptide molecules. Moreover, a stronger interaction with anionic lipids compared to the zwitterionic ones justified the model of the predominant electrostatic interaction to drive the peptide–lipid association. The implementation of the hybrid nanoplatforms from planar silica surfaces to 3D silica nanoparticles doped in the core with coumarin dye molecules allowed to demonstrate, by energy transfer processes, the actual wrapping of the nanoparticle by the peptide-associated supported lipid membrane. These proof-of-working experiments are very promising in view of the application in imaging and therapy of the developed nanoplatforms.

Cellular experiments highlighted the suitability of the NGF(1–14)-SLB systems as a non-toxic biointerface for neuronal cells. The maintenance of proliferative activity of NGF(1–14) associated with the supported membrane was proved in view of their application as functional nanoplatforms in cell adhesion and drug delivery.

Further investigations are in progress to optimize lipid composition/charge conditions for the association of the NGF(1–14) peptide fragment, the subsequent self-assembling process to form SLB-wrapped silica nanoparticles, as well as in-depth cellular assays.

Acknowledgements

The authors acknowledge MIUR (Italian Ministry for Research and University) grants FIRB ITALNANONET (RBPR05JH2P_021), PRIN 2010 (2010M2JARJ) and PON 01_01078.

Notes and references

1 W. T. Al-Jamal and K. Kostarelos, *Acc. Chem. Res.*, 2011, **44**, 1094.
2 (*a*) D. J. Irvine, *Nat. Mater.*, 2011, **10**, 342; (*b*) J. W. Liu, A. Stace-Naughton, X. M. Jiang and C. J. Brinker, *J. Am. Chem. Soc.*, 2009, **131**, 1354.
3 C. E. Ashley, E. C. Carnes, K. E. Epler, D. P. Padilla, J. K. Phillips, R. E. Castillo, D. C. Wilkinson, B. S. Wilkinson, C. A. Burgard, R. M. Kalinich, J. L. Townson, B. Chackerian, C. L. Willman, D. S. Peabody, W. Wharton and C. J. Brinker, *ACS Nano*, 2012, **6**, 2174.
4 V. Cauda, H. Engelke, A. Sauer, D. Arcizet, C. Bräuchle, J. Rädler and T. Bein, *Nano Lett.*, 2010, **10**, 2484.
5 (*a*) J. W. Liu, X. M. Jiang, C. Ashley and C. J. Brinker, *J. Am. Chem. Soc.*, 2009, **131**, 7567; (*b*) J. W. Liu, A. Stace-Naughton and C. J. Brinker, *Chem. Commun.*, 2009, 5100.
6 C. Satriano, S. Svedhem and B. Kasemo, *Phys. Chem. Chem. Phys.*, 2012, **14**, 16695.
7 C. Satriano, M. E. Fragalà, G. Forte, A. M. Santoro, D. La Mendola and B. Kasemo, *Soft Matter*, 2012, **8**, 53.
8 A. Travaglia, G. Arena, R. Fattorusso, C. Isernia, D. La Mendola, G. Malgieri, V. G. Nicoletti and E. Rizzarelli, *Chem.–Eur. J.*, 2011, **17**, 3726.
9 R. Levi-Montalcini, *Science*, 1987, **237**, 1154.
10 A. Travaglia, A. Pietropaolo, D. La Mendola, V. G. Nicoletti and E. Rizzarelli, *J. Inorg. Biochem.*, 2012, **111**, 130.
11 A. Cattaneo, S. Capsoni and F. Paoletti, *J. Alzheimers Dis.*, 2008, **15**, 255.
12 (*a*) Y. Cho, R. Shi, A. Ivanisevic and R. Ben Borgens, *Nanotechnology*, 2009, **8**, 20275102; (*b*) R. de Boer, A. M. Knight, R. J. Spinner, M. J. Malessy, M. J. Yaszemski and A. J. Windebank, *J. Biomed. Mater. Res., Part A*, 2010, **95**, 106.
13 L. C. Schecterson and M. Bothwell, *Dev. Neurobiol.*, 2010, **70**, 332.
14 M. Barbacid, *J. Neurobiol.*, 1994, **25**, 1386.
15 F. M. Longo and S. M. Massa, *J. Alzheimers Dis.*, 2004, **6**, S13.
16 T. Wehrman, X. He, B. Raab, A. Dukipatti, H. Blau and K. C. Garcia, *Neuron*, 2007, **53**, 25.
17 R. P. Richter, R. Bérat and A. R. Brisson, *Langmuir*, 2006, **22**, 3497.
18 S. Bonacchi, D. Genovese, R. Juris, M. Montalti, L. Prodi, E. Rampazzo and N. Zaccheroni, *Angew. Chem., Int. Ed.*, 2011, **50**, 4056.
19 L. Brancaleon, M. P. Bamberg, T. Sakamaki and N. Kollias, *J. Invest. Dermatol.*, 2001, **116**, 380.
20 D. M. Byler and H. Susi, *Biopolymers*, 1986, **25**, 469.
21 C. A. Keller and B. Kasemo, *Biophys. J.*, 1998, **75**, 1397.
22 F. F. Rossetti, M. Textor and I. Reviakine, *Langmuir*, 2006, **22**, 3467.
23 C. Satriano, M. Edvardsson, G. Ohlsson, G. Wang, S. Svedhem and B. Kasemo, *Langmuir*, 2010, **26**, 5715.
24 D. Axelrod, D. E. Koppel, J. Schlessinger, E. Elson and W. W. Webb, *Biophys. J.*, 1976, **16**, 1055.
25 G. M. Lee, A. Ishihara and K. A. Jacobson, *Proc. Natl. Acad. Sci. U. S. A.*, 1991, **88**, 6274.
26 S. Pautot, H. Lee, E. Y. Isacoff and J. T. Groves, *Nat. Chem. Biol.*, 2005, **1**, 283.
27 D. Afanasenkau and A. Offenhäusser, *Langmuir*, 2012, **28**, 13387.
28 E. Rampazzo, S. Bonacchi, D. Genovese, R. Juris, M. Sgarzi, M. Montalti, L. Prodi, N. Zaccheroni, G. Tomaselli, S. Gentile, C. Satriano and E. Rizzarelli, *Chem.–Eur. J.*, 2011, **17**, 13429.
29 T. Förster, *Discuss. Faraday Soc.*, 1959, **27**, 7.
30 E. Rampazzo, S. Bonacchi, R. Juris, M. Montalti, D. Genovese, N. Zaccheroni, L. Prodi, D. C. Rambaldi, A. Zattoni and P. Reschiglian, *J. Phys. Chem. B*, 2010, **114**, 14605.
31 M. Montalti, A. Credi, L. Prodi and M. T. Gandolfi, *Handbook of Photochemistry*, CRC Taylor & Francis, Boca Raton, FL, 3rd edn, 2006.